1242 *Chem. Mater.* **2010,** *22,* 1242–1248
DOI:10.1021/cm902720z

CHEMISTRY OF MATERIALS
Article

Anti-Site Defects and Ion Migration in the $LiFe_{0.5}Mn_{0.5}PO_4$ Mixed-Metal Cathode Material†

Grahame R. Gardiner and M. Saiful Islam*

Department of Chemistry, University of Bath, Bath BA2 7AY, U.K.

Received September 1, 2009. Revised Manuscript Received November 25, 2009

Olivine-type phosphates have attracted considerable attention as cathode materials for rechargeable lithium batteries. Here, the defect and ion transport properties of the mixed-metal material $LiFe_{0.5}Mn_{0.5}PO_4$ are investigated by atomistic modeling methods. The intrinsic defect type with the lowest energy is the cation antisite defect, in which Li and Fe/Mn ions exchange positions. As found in the $LiFePO_4$ material, lithium ion diffusion in the mixed-metal system occurs down the *b*-axis channels following a curved path. Migration energies for Fe and Mn antisite cations on Li sites suggest that Mn defects would impede bulk Li mobility in $LiFe_{0.5}Mn_{0.5}PO_4$ to a greater extent than Fe antisite defects in $LiFePO_4$. Association or binding energies for various defect clusters comprised of lithium vacancies and/or antisite cations are examined.

1. Introduction

In the field of energy storage research, there is considerable activity devoted to finding new cathode materials for next-generation lithium batteries, particularly for potential use in hybrid electric or pure electric vehicles.[1,2] The olivine-structured compound $LiFePO_4$ has become a highly studied and commercially viable alternative to the conventional cathode material, $LiCoO_2$.[3−10] Attention also continues to be paid to the other transition metal phosphates, such as $LiMnPO_4$, largely due to the higher cell voltages than $LiFePO_4$.

As with the layered-oxide cathodes (for example, $LiNi_{0.5}Mn_{0.5}O_2$), there have been investigations of solid-solutions or mixed-metal phosphates, especially the $LiFe_{1-y}Mn_yPO_4$ and $LiFe_{0.5}Mn_{0.5}PO_4$ materials.[3,11−15] The early work of Padhi et al.[3] showed that solid solutions of $LiFe_{1-y}Mn_yPO_4$ allowed access to the Mn^{3+}/Mn^{2+} couple for $y < 0.75$. These mixed-metal phosphates are isostructural with their $LiFePO_4$ and $LiMnPO_4$ end-members, adopting the same olivine-type lattice. Yamada et al.[11] carried out extensive studies of $LiFe_{1-y}Mn_yPO_4$ and found that pure $MnPO_4$ is an intrinsically unstable compound. This was attributed to Jahn−Teller distortions around trivalent Mn, making Mn-rich phases far from practical application. Delacourt et al.[5] also showed that $LiMnPO_4$ has lower electrical conductivity by several orders of magnitude than $LiFePO_4$, and Zaghib et al.[15] used FTIR and magnetometry to investigate the local structures of $Li_xFe_{0.5}Mn_{0.5}PO_4$ phases.

The possibility of improved energy density over $LiFePO_4$ has therefore generated continued interest in the olivine-type mixed system $LiFe_{1-y}Mn_yPO_4$. However, the optimum Fe/Mn composition is still yet to be determined. To understand the local structural features influencing the electrochemical behavior of mixed-metal phosphates, it is clear that fundamental knowledge of their underlying defect and transport properties is needed on the atomic scale. Atomistic simulation techniques provide a powerful means of investigating these key solid-state issues, but have not been applied to mixed-metal phosphate materials.

† Accepted as part of the 2010 "Materials Chemistry of Energy Conversion Special Issue".

*Author to whom correspondence should be addressed. Fax: +44-(0)1225-386231. E-mail: m.s.islam@bath.ac.uk.

(1) Tarascon, J.-M.; Armand, M. *Nature* **2008**, *451*, 652.
(2) Whittingham, M. S. *Chem. Rev.* **2004**, *104*, 4271.
(3) (a) Padhi, A. K.; Nanjundaswamy, K. S.; Goodenough, J. B. *J. Electrochem. Soc.* **1997**, *144*, 1188. (b) Padhi, A. K.; Nanjundaswamy, K. S.; Masquelier, C.; Goodenough, J. B. *J. Electrochem. Soc.* **1997**, *144*, 2581.
(4) Howard, W. F.; Spotnitz, R. M. *J. Power Sources* **2007**, *165*, 887.
(5) Delacourt, C.; Laffont, L.; Bouchet, R.; Wurm, C.; Leriche, J.-B.; Morcrette, M.; Tarascon, J.-M.; Masquelier, C. *J. Electrochem. Soc.* **2005**, *152*, A913.
(6) Kang, B.; Ceder, G. *Nature*. **2009**, *458*, 190.
(7) Delmas, C.; Maccario, M.; Croguennec, L.; Le Cras, F.; Weill, F. *Nat. Mater.* **2008**, *7*, 665.
(8) Axmann, P.; Stinner, C.; Wohlfahrt-Mehrens, M.; Mauger, A.; Gendron, F.; Julien, C. M. *Chem. Mater.* **2009**, *21*, 1636.
(9) Meethong, N.; Kao, Y.; Speakman, S. A.; Chiang, Y. M. *Adv. Funct. Mater.* **2009**, *19*, 1.
(10) Ellis, B.; Subramanya Herle, P.; Rho, Y.-H.; Nazar, L. F.; Dunlap, R.; Perry, L. K.; Ryan, D. H. *Faraday Discuss.* **2007**, *134*, 119.
(11) (a) Yamada, A.; Kudo, Y.; Liu, K. *J. Electrochem. Soc.* **2001**, *148*, A747. (b) Yamada, A.; Chung, S. *J. Electrochem. Soc.* **2001**, *148*, A960.
(12) Fang, H.; Pan, Z.; Li, L.; Yang, Y.; Yan, G.; Li, G.; Wei, S. *Electrochem. Commun.* **2008**, *10*, 1071.
(13) (a) Molenda, J.; Ojczyk, W.; Świerczek, K.; Zając, W.; Krok, F.; Dygas, J.; Liu, R.-S. *Solid State Ionics* **2006**, *177*, 2617. (b) Molenda, J.; Qjczyk, W.; Marzec, J. *J. Power Sources* **2007**, *174*, 689.
(14) Burba, C. M.; Frech, R. *J. Power Sources* **2007**, *172*, 870.
(15) (a) Zaghib, K.; Mauger, A.; Gendron, F.; Massot, M.; Julien, C. M. *Ionics* **2008**, *14*, 371. (b) Gwon, H.; Seo, D. H.; Kim, S. W.; Kim, J.; Kang, K. *Adv. Funct. Mater.* **2009**, *19*, 3285.

Published on Web 12/22/2009

The present work focuses on the $LiFe_{0.5}Mn_{0.5}PO_4$ composition and extends our previous simulation studies of the $LiFePO_4$ material[16,17] and, more recently, the Li_2MnSiO_4 system.[18] Here we present a study on the energetics of intrinsic disorder, defect association, Li migration and antisite cation migration in the $LiFe_{0.5}Mn_{0.5}PO_4$ mixed-metal battery material.

2. Computational Techniques

This study uses well established modeling techniques, which are detailed elsewhere,[19] and hence only a general description will be given here. Interactions between ions in the mixed-metal phosphate consist of a long-range Coulombic term and a short-range component representing electron−electron repulsion and van der Waals interactions. The short-range interactions were modeled using the two-body Buckingham potential, and an additional three-body term was used for the PO_4 units to take into account the angle-dependent nature of O—P—O bonds, as used previously for $LiFePO_4$.[16,17] Such three-body terms have also been applied successfully to simulations of aluminophosphates[20] and olivine silicates.[21] The effects of electronic polarization are treated by the shell model,[19] which has proven effective in simulating dielectric properties of a wide range of ceramic oxides.

The long-range lattice relaxation about point defects, defect clusters or migrating ions was calculated using an implementation of the Mott−Littleton method incorporated in the GULP code.[22] This method partitions the crystal lattice into two regions, with ions within the inner spherical region surrounding the defect relaxed explicitly, and a continuum treatment of the outer region. In this study, lattice supercells of the inner and outer regions contained 1160 and 8265 ions respectively. It should be noted that relaxation of such a large number of ions is important for charged defects that introduce long-range electrostatic perturbations, and is not easily treated by electronic structure methods such as DFT.

The calculated energies of isolated charged defects (such as Li^+ vacancies) from the Mott−Littleton method relate to minimizing the potential energy function of the defective static lattice with respect to the displacements of the surrounding ions. The energy difference between the potential energy for the perfect lattice and the lattice containing the point defect gives the corresponding defect formation energy. This energy of an isolated charged defect is combined with other defect energies to derive total energies for charge-balanced defect reactions, for example, Schottky or Frenkel formation energies. These calculated reaction energies can then be compared directly with experimental data (if available), and indeed have generally found good quantitative agreement for a range of halides and oxides.[19] These methods have also been employed successfully on a wide-range of other complex oxides, including recent work on the $LaBaGaO_4$ fuel cell electrolyte,[23] and earlier studies on lithium insertion into TiO_2 and Fe_3O_4.[24]

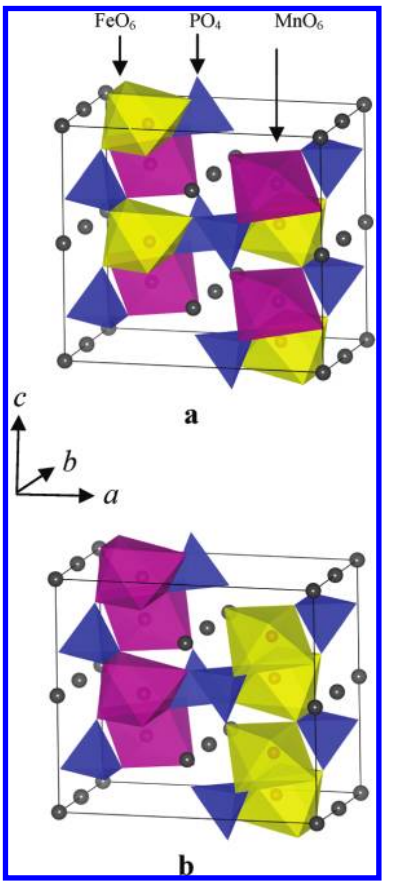

Figure 1. Olivine-type structure of $LiFe_{0.5}Mn_{0.5}PO_4$ showing two Fe/Mn cation ordering configurations: (a) FeO_6 and MnO_6 octahedra alternating regularly; (b) separate $\{FeO_6\}$ and $\{MnO_6\}$ planes.

The starting point of the present study was to reproduce the experimentally observed crystal structure.[25,26] All of the interatomic potentials were taken from our previous work on $LiMPO_4$.[16] As with the $LiFePO_4$ and $LiMnPO_4$ end-members, the olivine structure exhibited by $LiFe_{0.5}Mn_{0.5}PO_4$ is orthorhombic (space group *Pnma*), and consists of PO_4 tetrahedra with both Fe and Mn ions on corner-sharing octahedral positions (4*c* sites in Wyckoff notation) and Li^+ ions on edge-sharing octahedral positions (4*a* sites), the latter running parallel to the *b* axis.

(16) (a) Islam, M. S.; Driscoll, D. J.; Fisher, C. A. J.; Slater, P. R. *Chem. Mater.* **2005**, *17*, 5085. (b) Fisher, C. A. J.; Hart-Prieto, V. M.; Islam, M. S. *Chem. Mater.* **2008**, *20*, 5907.
(17) Fisher, C. A. J.; Islam, M. S. *J. Mater. Chem.* **2008**, *18*, 1209.
(18) Kuganathan, N.; Islam, M. S. *Chem. Mater.* **2009**, *21*, 5196.
(19) Catlow, C. R. A. *Computer Modelling in Inorganic Crystallography*; Academic Press: San Diego, 1997.
(20) Henson, N. J.; Cheetham, A.; Gale, J. D. *Chem. Mater.* **1996**, *8*, 664.
(21) Walker, A. M.; Wright, K.; Slater, B. *Phys. Chem. Miner.* **2003**, *30*, 536.
(22) Gale, J. D.; Rohl, A. L. *Mol. Simul.* **2003**, *29*, 291.
(23) Kendrick, E.; Kendrick, J.; Knight, K. S.; Islam, M. S.; Slater, P. R. *Nat. Mater.* **2007**, *6*, 871.
(24) (a) Olson, C. L.; Nelson, J.; Islam, M. S. *J. Phys. Chem. B* **2006**, *110*, 9995. (b) Islam, M. S.; Catlow, C. R. A. *J. Solid State Chem.* **1988**, *77*, 180.
(25) (a) García-Moreno, O.; Alvarez-Vega, M.; García-Alvarado, F.; García-Jaca, J.; Gallardo Amores, J. M.; Sanjuán, M. L.; Amador, U. *Chem. Mater.* **2001**, *13*, 1570. (b) Rousse, G.; Rodriguez-Carvajal, J.; Patoux, S.; Masquelier, C. *Chem. Mater.* **2003**, *15*, 4082.
(26) Losey, A.; Rakovan, J.; Hughes, J. M.; Francis, C. A.; Dyar, M. D. *Can. Mineral.* **2004**, *42*, 1105.

The initial structural parameters were based on recent diffraction studies of the Li(Fe,Mn)PO_4 system.[26] For structural modeling, two main configurations of the Fe^{2+}/Mn^{2+} cations in $LiFe_{0.5}Mn_{0.5}PO_4$ were explored (as illustrated in Figure 1). Figure 1a shows intraplanar ordering in which FeO_6 and MnO_6 octahedra alternate regularly within the same bc plane; and Figure 1b shows interplanar ordering consisting of separate {FeO_6} and {MnO_6} planes. The energetics of these structures were investigated by performing a series of geometry optimizations in P1 symmetry. Our results indicate that the lowest energy structure is the configuration in which Fe and Mn alternate within the same plane (shown in Figure 1a). However, we note that the lattice energy differences were found to be very small (< 50 meV), which is consistent with current diffraction studies suggesting no significant cation ordering.[3,26] We recognize that further structural work is necessary to elucidate whether Fe/Mn ordering occurs in $LiFe_{0.5}Mn_{0.5}PO_4$, which may depend on synthesis routes.

Using the lowest energy structure, a comparison between the calculated and experimental crystal structures are given in Table 1. The calculated unit cell parameters and cation-oxygen bond lengths for $LiFe_{0.5}Mn_{0.5}PO_4$ deviate from experiment by at most 0.07 Å, and in most cases much less. This gives us confidence that the interatomic potential model can be used reliably in subsequent defect, cluster and migration calculations.

3. Results and Discussion

3.1. Intrinsic Defects. A series of isolated point defect (vacancy and interstitial) energies were first calculated, and then combined to give the relative energies of formation of Frenkel and Schottky-type defects in $LiFe_{0.5}Mn_{0.5}PO_4$. These take the following general forms (using Kröger−Vink notation and where $M = Mn^{2+}, Fe^{2+}$):

$$\text{Li Frenkel} : \mathrm{Li}_{\mathrm{Li}}^{\times} \rightarrow \mathrm{V}_{\mathrm{Li}}' + \mathrm{Li}_i^{\bullet} \quad (1)$$

$$M\text{Frenkel} : M_M^{\times} \rightarrow \mathrm{V}_M'' + \mathrm{M}_i'' \quad (2)$$

$$\text{O Frenkel} : \mathrm{O}_{\mathrm{O}}^{\times} \rightarrow \mathrm{V}_{\mathrm{O}}^{\bullet\bullet} + \mathrm{O}_i'' \quad (3)$$

$$\text{Schottky} : \mathrm{Li}_{\mathrm{Li}}^{\times} + \frac{1}{2}\mathrm{Fe}_{\mathrm{Fe}}^{\times} + \frac{1}{2}\mathrm{Mn}_{\mathrm{Mn}}^{x} + \mathrm{P}_{\mathrm{P}}^{\times} + 4\mathrm{O}_{\mathrm{O}}^{\times} \rightarrow \mathrm{V}_{\mathrm{Li}}^{\times} + \frac{1}{2}\mathrm{V}_{\mathrm{Fe}}'' + \frac{1}{2}\mathrm{V}_{\mathrm{Mn}}'' + \mathrm{V}_{\mathrm{P}}'''' + 4\mathrm{V}_{\mathrm{O}}^{\cdot\cdot} + \mathrm{LiFe}_{0.5}\mathrm{Mn}_{0.5}\mathrm{PO}_4 \quad (4)$$

$$\mathrm{Li_2O\ Schottky\text{-}like} : 2\mathrm{Li}_{\mathrm{Li}}^{\times} + \mathrm{O}_{\mathrm{O}}^{\times} \rightarrow 2\mathrm{V}_{\mathrm{Li}}' + \mathrm{V}_{\mathrm{O}}^{\bullet\bullet} + \mathrm{Li_2O} \quad (5)$$

$$M\text{O Schottky-like} : M_M^{\times} + \mathrm{O}_{\mathrm{O}}^{\times} \rightarrow \mathrm{V}_M'' + \mathrm{V}_{\mathrm{O}}^{\bullet\bullet} + M\mathrm{O} \quad (6)$$

As with our earlier study on $LiFePO_4$,[16] we also examined the Li/M "anti-site" pair defect, which involves the exchange of an Li^+ ion (radius 0.74 Å) with an M^{2+} ion (Mn^{2+} radius 0.83 Å or Fe^{2+} radius 0.78 Å) according to:

$$\mathrm{Li}_{\mathrm{Li}}^{\times} + M_M^{\times} \rightarrow \mathrm{Li}_M' + M_{\mathrm{Li}}^{\bullet} \quad (7)$$

Finally, off-stoichiometry defects involving lithium deficiency and increased oxidation state of the transition-metal cation was also considered according to

$$\mathrm{Li}_{\mathrm{Li}}^{\times} + \frac{1}{4}\mathrm{O}_2 \rightarrow \mathrm{V}_{\mathrm{Li}}' + h^{\bullet} + \frac{1}{2}\mathrm{Li_2O} \quad (8)$$

Our approach to electronic defects follows that used for other transition-metal oxides[24] in which we model the localized hole ($h^{\bullet}$) species (small polaron) on the transition metal ion as M^{3+}. With regard to the hole species, our calculations found that the initial formation of Mn^{3+} species is more favorable than Fe^{3+} by about 2 eV, although we recognize that there will be significant 3d−O2p mixing. Our concern here is to understand key trends in these defect reactions, a task for which our modeling methods have proven to be reliable.

As with previous simulation studies, the total energies of all these defect reactions (eqs 1−8) are derived by using the calculated energies of the corresponding isolated defects. For example, the total energy for reaction 7 is the sum of the energies of the two antisite cations as isolated defects. We note that for the Frenkel defect reactions, possible interstitial defect sites within the structure were explored with the lowest energy positions used (listed in the Supporting Information).

Examination of the results in Table 2 reveals two main findings. First, the magnitude of the calculated energies suggests formation of Frenkel and Schottky defects is unfavorable. The intrinsic redox process with V_{Li}' and M^{3+} formation is also unfavorable, which is consistent with the observation that these materials exhibit low

Table 1. Calculated and Experimental[26] Structural Parameters of $LiFe_{0.5}Mn_{0.5}PO_4$

(a) Unit Cell Parameters

parameter	calc/Å	expt/Å	Δ/Å
a	10.4571	10.3826	0.0745
b	6.0556	6.0499	0.0057
c	4.6786	4.7138	−0.0352

(b) Bond Lengths

ion pair	calc/Å	expt/Å	Δ/Å
P—O(1)	1.511	1.522	−0.011
P—O(2)	1.554	1.538	0.016
P—O(3)	1.572	1.552	0.020
Li—O(1)	2.209	2.199	0.010
Li—O(2)	2.104	2.092	0.012
Li—O(3)	2.228	2.173	0.055
Fe—O(1)	2.209	2.223	−0.014
Fe—O(2)	2.062	2.122	−0.060
Fe—O(3)	2.055	2.095	−0.040
Fe—O(3)	2.235	2.261	−0.026
Mn—O(1)	2.208	2.223	−0.015
Mn—O(2)	2.096	2.122	−0.026
Mn—O(3)	2.104	2.095	0.009
Mn—O(3)	2.262	2.261	0.001

Table 2. Energies of Intrinsic Defect Processes in $LiFe_{0.5}Mn_{0.5}PO_4$

defect	equation	energy (eV)
Li Frenkel	1	2.75
Fe Frenkel	2	6.71
Mn Frenkel	2	6.84
O Frenkel	3	6.00
Full Schottky	4	28.38
Li_2O Shottky-type	5	6.53
FeO Schottky-type	6	5.98
MnO Schottky-type	6	6.23
Li/Fe Antisite	7	1.22
Li/Mn Antisite	7	1.34
Li+ deficiency	8	4.69

intrinsic electronic conduction, and that they do not show large deviations from stoichiometry.

Second, the most favorable intrinsic defect for the $LiFe_{0.5}Mn_{0.5}PO_4$ material is the Li/M antisite pair, as predicted in our earlier study of $LiFePO_4$.[16] This suggests that even at low temperatures there will be a small percentage (~1%) of Fe or Mn ions on Li sites with a slightly lower energy for the Li/Fe antisite defect. The concentration of such defects would be temperature dependent and hence sensitive to experimental synthesis conditions and thermal history.

We note that due to uncertainties in the precise mass-action relations for the phosphate compositions it is difficult to predict the exact concentration of such defects at high temperatures. Nevertheless, structural analysis of hydrothermally synthesized $LiFePO_4$ suggests 3 mol % Fe on the lithium sites,[27] whereas a recently reported scanning transmission electron microscopy (STEM) study[28] confirms our earlier prediction of antisite defects in $LiFePO_4$, quoting a concentration of around 1%. Diffraction and EXAFS studies[12] of $LiMnPO_4$ find Mn^{2+} disorder on Li^+ sites. Axmann et al.[8] also find a few at.% Fe on Li sites in $LiFePO_4$, but not Li on Fe sites. More recently, Hamelet et al.[29] have found Li−Fe exchange in $LiFePO_4$-based nano powders with significant amounts of structural defects.

3.2. Defect Clusters. It is well established that the electrostatic and elastic interactions between point defects can lead to their clustering or association. Indeed, the defect chemistry and possible association (trapping) in $LiFePO_4$ have been discussed recently by Maier and Amin,[30] where they note that detailed atomistic modeling is required to quantify the energies of association. As demonstrated by previous studies on complex oxides,[31] our simulation methods can model accurately the electrostatic, polarization and elastic strain energies, which are the predominant terms in any local association process. The clusters considered in the $LiFe_{0.5}Mn_{0.5}PO_4$ system are comprised of combinations of antisite defects and lithium vacancies.

(27) Chen, J.; Vacchio, M. J.; Wang, S.; Chernova, N.; Zavalij, P. Y.; Whittingham, M. S. *Solid State Ionics* **2008**, *178*, 1676.
(28) Chung, S.-Y.; Choi, S.-Y.; Yamamoto, T.; Ikuhara, Y. *Phys. Rev. Lett.* **2008**, *100*, 125502.
(29) Hamelet, S.; et al. *J. Mater. Chem.* **2009**, *19*, 3979.
(30) Maier, J.; Amin, R. *J. Electrochem. Soc.* **2008**, *155*, A339.
(31) (a) Mather, G. C.; Islam, M. S.; Figueirido, F. M. A. *Adv. Funct. Mater.* **2007**, *17*, 905. (b) Islam, M. S.; Davies, R. A. *J. Mater. Chem.* **2004**, *14*, 86.

Table 3. Binding Energies of Defect Pair Clusters on Neighboring Cation Sites in $LiFePO_4$, $LiFe_{0.5}Mn_{0.5}PO_4$ and $LiMnPO_4$

	E_{bind}/eV		
defect cluster	$LiFePO_4$	$LiFe_{0.5}Mn_{0.5}PO_4$	$LiMnPO_4$
$[Li_{Fe}'-Fe_{Li}^{\bullet}]$	−0.44	−0.46	
$[Li_{Mn}'-Fe_{Mn}^{\bullet}]$		−0.49	−0.57
$[Fe_{Li}^{\bullet}-V_{Li}']$	−0.48	−0.52	
$[Mn_{Li}^{\bullet}-V_{Li}']$		−0.54	−0.65

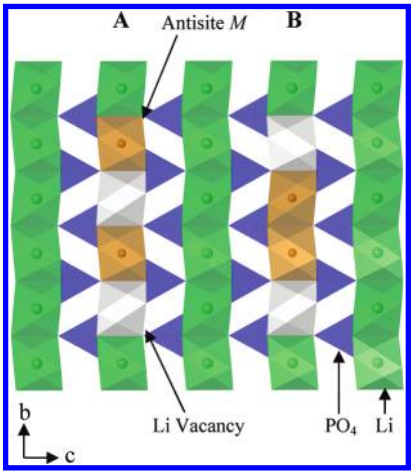

Figure 2. Schematic of the structural plane showing two different neutral cluster configurations along the *b*-axis lithium channel comprised of two antisite defects (Fe or Mn ions on Li sites) and two Li vacancies: (A) antisite cation and Li vacancy at alternating sites (B) antisite cations at adjacent sites.

The cluster binding energies (E_{bind}) were calculated using the general relation

$$E_{bind} = E_{cluster} - \sum_{component} E_{isolated} \quad (9)$$

where a negative value indicates that the cluster is stable with respect to the isolated component defects. First, energies of pairs of defects on neighboring cation sites were calculated relative to the same number of isolated defects. The two types of defect pair cluster considered were Li/M antisite defects, $[Li_M'-M_{Li}^{\bullet}]$, and M^{2+} on an Li site neighboring a Li vacancy, $[M_{Li}^{\bullet}-V_{Li}']$ where M = Fe or Mn. The corresponding binding energies are listed in Table 3 for $LiFe_{0.5}Mn_{0.5}PO_4$, as well as the end-members, $LiFePO_4$ and $LiMnPO_4$, for comparison.

We also considered larger neutral clusters comprised of two antisite cations ($M_{Li}^{\bullet}$) and two Li vacancies at neighboring sites along the *b* axis Li channel. The two different configurations examined (shown in Figure 2) have either alternating antisite and vacancy defects or two antisite defects at adjacent sites. The lowest binding energies for these neutral one-dimensional clusters are listed in Table 4.

Three key points can be identified from the results. First, both Li/Fe and Li/Mn antisite pair clusters have similar negative binding energies (Table 3), indicating that they are more stable than the isolated defects. This suggests that antisite defects will aggregate in the material, acting as possible precursors to larger clusters. Defect aggregation has been observed by STEM in $LiFePO_4$.[28]

Table 4. Binding Energies of Neutral Clusters Along the b axis Channel (shown in Figure 2)

cluster configuration	E_{bind} (per defect pair)/eV		
	$LiFePO_4$	$LiFe_{0.5}Mn_{0.5}PO_4$	$LiMnPO_4$
$[2Fe_{Li}^{\bullet} - 2\,V_{Li}']$			
a	−0.63	−0.66	
b	−0.42	−0.43	
$[2Mn_{Li}^{\bullet} - 2\,V_{Li}']$			
a		−0.69	−0.81
b		−0.44	−0.55

However, the latter study of Chung at al[28] does not clearly indicate the precise compensation mechanism for the possible supervalent Nb doping, since the antisite cations ($Fe_{Li}^{\bullet}$) also have effective positive charges. It is worth noting that our simulations find that clusters of only $Fe_{Li}^{\bullet}$ antisite defects on neighboring sites always lead to positive binding energies, which indicate unfavorable interactions between such like-charged defects.

Second, the results reveal significant binding between antisite defects ($M_{Li}^{\bullet}$) and Li vacancies. The cluster configuration with the strongest binding energy (> −0.6 eV) is found for the larger one-dimensional cluster (A) shown in Figure 2. This arrangement seems to minimize the repulsive interactions between like-charged antisite cations.

Finally, such Fe or Mn ions on the lithium site ($M_{Li}^{\bullet}$) could lead to trapping of the migrating Li^+ vacancies, which would hinder lithium diffusion along the *b*-axis channel. Our results agree well with recent structural studies of Axmann et al.[8] who find that the antisite $Fe_{Li}^{\bullet}$ defect is not isolated but coupled to a Li vacancy to form a complex $Fe_{Li}^{\bullet} + V_{Li}'$.

In general, these results suggest aggregation or clustering of defects (rather than a random distribution), which may be important as precursors to local ordering or nanodomain formation, and warrants further investigation. Such clustering may inhibit Li extraction in which defect cluster regions are more likely to retain lithium.

3.3. Li Ion and Anti-Site Cation Migration. As performed previously on $LiFePO_4$,[16] atomistic simulation techniques can be used to examine various possible ion diffusion paths and their energetics. First, three possible lithium migration paths in $LiFe_{0.5}Mn_{0.5}PO_4$ were examined, and are shown in Figure 3. Path A involves migration between adjacent Li sites in the [010] direction, that is, parallel to the *b* axis, with a jump distance of 2.9−3.0 Å. Path B involves migration in the [001] direction, with a jump distance of 4.6−4.7 Å, while path C involves migration between the lithium channels in the [101] direction with the longest jump distance of 5.6−5.8 Å.

Energy profiles for these mechanisms can be derived by calculating the energy of the migrating ion along the diffusion path, after relaxing the surrounding ions. At each point the migrating Li ion is allowed to relax in directions orthogonal to the direct linear path. The position of highest potential energy along the migration path corresponds to the activation energy of migration, E_{mig}. The migration energies for the $LiFe_{0.5}Mn_{0.5}PO_4$ system (as well as the $LiFePO_4$ and $LiMnPO_4$ for comparison) are listed in Table 5.

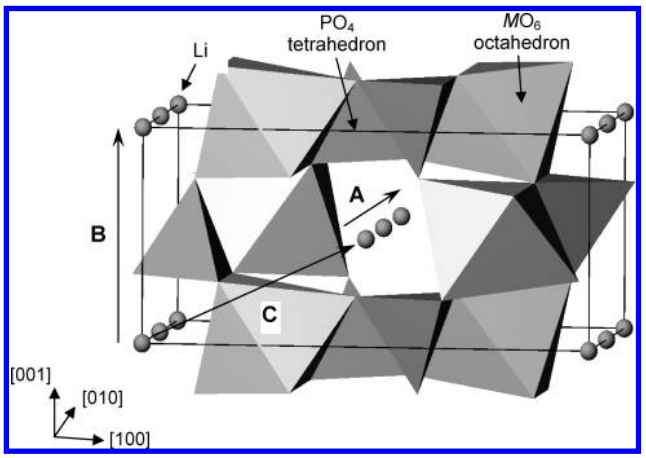

Figure 3. Paths considered for lithium ion migration in olivine-structured $LiFe_{0.5}Mn_{0.5}PO_4$.

Table 5. Energies and Pathways for Li Migration (Shown in Figure 3)

path	*E* mig /eV		
	$LiFePO_4$	$LiFe_{0.5}Mn_{0.5}PO_4$	$LiMnPO_4$
A [010]	0.55	0.59	0.62
B [001]	2.89	2.86	2.83
C [101]	3.36	3.58	2.26

The results reveal that the lowest energy path for Li ion migration in $LiFe_{0.5}Mn_{0.5}PO_4$ is down the [010] channel, path A, as found previously for $LiFePO_4$.[16,32] High barriers of > 2.2 eV are calculated for the other pathways (B and C), indicating that lithium ions cannot readily jump from one channel to another. This strongly confirms the anisotropic nature of Li ion migration in the olivine phosphates. Our calculated energy of 0.59 eV for $LiFe_{0.5}Mn_{0.5}PO_4$ agrees well with the experimental activation energy of 0.63 eV for mixed-metal $LiFe_{0.45}Mn_{0.55}PO_4$.[13]

We recognize that direct comparison with conductivity measurements is not straightforward. It has been suggested that Li motion in these materials is, to a greater or lesser extent, coupled to electron (small polaron) mobility,[33] although there is no direct evidence. Mossbauer studies of Ellis et al.[33] indicate that the onset of rapid small polaron hopping in Li_xFePO_4 is correlated with the temperature that the lithium ions begin to disorder in the lattice.

Detailed local structural analysis of our simulation data shows that a curved migration path is taken between the adjacent lithium sites (shown in Figure 4), and not a direct linear path. The maximum deviation from the linear path is calculated to be 0.44 Å, which is very similar to the value (0.5 Å) found for $LiFePO_4$. More recently, by using neutron diffraction and the maximum entropy method, Yamada and co-workers[34] confirm one-dimensional Li^+ diffusion in Li_xFePO_4, with a curved migration

(32) Morgan, D.; Van der Ven, A.; Ceder, G. *Electrochem. Solid State Lett*. **2004**, *7*, A30.
(33) (a) Ellis, B.; Perry, L. K.; Ryan, D. H.; Nazar, L. F. *J. Am. Chem. Soc*. **2006**, *128*, 11416. (b) Maxisch, T.; Zhou, F.; Ceder, G. *Phys. Rev. B*. **2006**, *73*, 104301.
(34) Nishimura, S; Kobayashi, G.; Ohayama, K; Kanno, R.; Yashima, M.; Yamada, A. *Nat. Mater*. **2008**, *7*, 707.

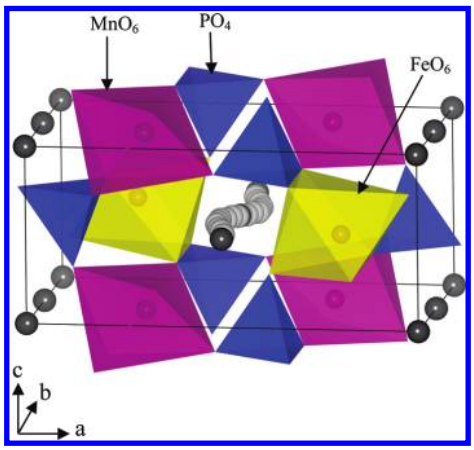

Figure 4. Curved migration pathway calculated for lithium ion transport along the *b* axis in $LiFe_{0.5}Mn_{0.5}PO_4$ (as found in $LiFePO_4$ (ref 16)).

pathway between adjacent lithium sites, in excellent agreement with the present simulation results, as well as our earlier prediction.[16]

These results contrast with a recent report that lithium ion diffusion in single crystals of $LiFePO_4$ was two rather than one-dimensional.[35] However, two-dimensional transport with similar activation energies in the *b* and *c* directions is difficult to reconcile with the distinctly anisotropic nature of the orthorhombic olivine structure; for example, the corresponding Li−Li jump distances are highly disparate at 2.9−3.0 Å and 4.6−4.7 Å respectively. More recently, Li et al.[36] find different results on single crystal $LiFePO_4$ with lithium diffusion confined to one-dimension through the *b*-axis tunnels.

Our defect calculations suggest that Li/Fe and Li/Mn antisite defects are intrinsic to $LiFe_{0.5}Mn_{0.5}PO_4$. In order to examine whether antisite defects affect long-range Li diffusion, the energy of migration of the divalent antisite cation between lithium sites was calculated. This process can be viewed as an exchange of an antisite cation ($M_{Li}^{\bullet}$) with a lithium vacancy (as illustrated in Figure 5), in which the lithium vacancy would then continue to migrate in the opposite direction down the [010] channel. The transition state (saddle-point) configuration for such migration has the antisite cation midway between the two vacant Li (4a) sites, with no significant differences in position for the migrating Fe or Mn antisite defects.

All the calculated migration energies in Table 6 are about 0.2−0.3 eV greater than the corresponding Li migration values, indicating lower Fe or Mn antisite cation mobility compared to pure lithium diffusion. This suggests that such antisite defects ($M_{Li}^{\bullet}$) would impede Li diffusion to varying degrees down [010] channels. However, the higher antisite migration energy (0.87 eV) in $LiFe_{0.5}Mn_{0.5}PO_4$ compared to $LiFePO_4$, suggests that a population of antisite defects in this mixed-metal system would have a greater effect on lithium diffusion kinetics. This area warrants further investigation related

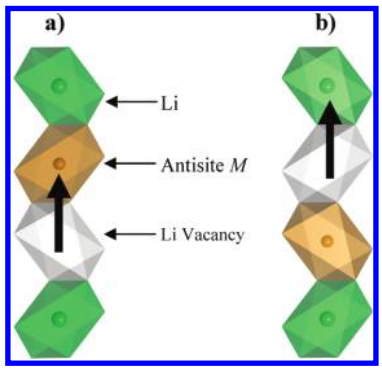

Figure 5. Schematic of two stages in the migration of an antisite cation ($M_{Li}^{\bullet}$) near a lithium vacancy ($V_{Li}^{'}$) down a [010] channel: (a) exchange of a lithium vacancy and an antisite cation (b) exchange of the lithium vacancy and a lithium ion.

Table 6. Energies of Anti-Site Cation Migration along [010] Channel (shown in Figure 5)

	E mig /eV		
mechanism	$LiFePO_4$	$LiFe_{0.5}Mn_{0.5}PO_4$	$LiMnPO_4$
$Fe_{Li}^{\bullet} \rightarrow V_{Li}^{'}$	0.70	0.79	
$Mn_{Li}^{\bullet} \rightarrow V_{Li}^{'}$		0.87	0.92

to recent experimental studies on the Li(Fe,Mn)PO_4 system.[37−39]

4. Conclusions

This investigation of the $LiFe_{0.5}Mn_{0.5}PO_4$ mixed-metal material has used atomistic simulation techniques to provide insights into the local defect chemistry and ion transport properties relevant to its electrochemical behavior.

Three key points emerge from the results. First, the most favorable intrinsic defect is the antisite defect, for which a small population (<2%) of Li^+ and Fe^{2+} or Mn^{2+} ions is expected to exchange sites. This would be temperature dependent and hence sensitive to experimental synthesis conditions. As in $LiFePO_4$, lithium ion diffusion in $LiFe_{0.5}Mn_{0.5}PO_4$ follows a nonlinear, curved path down the [010] channel; the migration energy (~0.6 eV) agrees with experimental data, and is intermediate between the two end members ($LiFePO_4$ and $LiMnPO_4$).

Second, the binding energies suggest clustering of defects (rather than a random distribution), which may be important as precursors to local ordering or nanodomain formation. Significant binding energies (> −0.6 eV) are found for neutral one-dimensional clusters along the *b*-axis channel comprised of antisite defects ($Fe_{Li}^{\bullet}$ or

(35) Amin, R.; Balaya, P.; Maier, J. *Electrochem. Solid-State Lett.* **2007**, *10*, A13.
(36) Li, J.; Yao, W.; Martin, S.; Vaknin, D. *Solid State Ionics* **2008**, *179*, 2016.
(37) (a) Kobayashi, G.; Yamada, A.; Nishimura, S.; Kanno, R.; Kobayashi, Y.; Seki, S.; Ohno, Y.; Miyashiro, H. *J. Power Sources* **2009**, *189*, 397. (b) Baek, D. H.; Kim, J. K.; Shin, Y. J.; Chauhan, G. S.; Ahn, J. H.; Kim, K. W. *J. Power Sources* **2009**, *189*, 59.
(38) (a) Chen, Y. C.; Chen, J. M.; Hsu, C. H.; Lee, J. F.; Yeh, J. W.; Shih, H. C. *Solid State Ionics* **2009**, *180*, 1215. (b) Kim, J. K.; Chauhan, G. S.; Ahn, J. H.; Ahn, H. J. *J. Power Sources* **2009**, *189*, 391. (c) Shin, Y. J.; Kim, J. K.; Cheruvally, G.; Ahn, J. H.; Kim, K. W. *J. Phys. Chem. Solids* **2008**, *69*, 1253.
(39) (a) Chen, G. Y.; Richardson, T. J. *J. Electrochem. Soc.* **2009**, *156*, A541. (b) Murugan, A. V.; Muraliganth, T.; Manthiram, A. *Inorg. Chem.* **2009**, *156*, A79.

$Mn_{Li}^{\bullet}$) and Li vacancies. This has implications for lithium conductivity as Fe or Mn cations on Li sites could lead to trapping of the migrating Li^{+} vacancies. Defect clustering therefore may inhibit Li extraction, in which defect cluster regions are more likely to retain lithium.

Finally, the higher antisite ($M_{Li}^{\bullet}$) migration energy in $LiFe_{0.5}Mn_{0.5}PO_4$ compared to pure $LiFePO_4$, suggests that any antisite defects in this mixed-metal system would have a greater blocking effect on lithium insertion/extraction rates.

Acknowledgment. We thank the EPSRC for funding as part of the Supergen Energy Storage Consortium (grant code EP/D031672/1), and the Materials Chemistry Consortium for HPCx and Hector supercomputer facilities. Crystal structure figures were produced using the VESTA code.[40]

Supporting Information Available: List of interstitial defect positions. This material is available free of charge via the Internet at http://pubs.acs.org.

(40) Momma, K.; Izumi, F. *J. Appl. Crystallogr.* **2008**, *41*, 653.